Spectrochimica Acta Part B: Atomic Spectroscopy 190 (2022) 106390

Contents lists available at ScienceDirect

Spectrochimica Acta Part B: Atomic Spectroscopy

journal homepage: www.elsevier.com/locate/sab

A critical evaluation of the chlorine quantification method based on molecular emission detection in LIBS

Luis Javier Fernández-Menéndez [a], Cristina Méndez-López [a], Carlos Abad [b], Jonatan Fandiño [a], Cristina González-Gago [a], Jorge Pisonero [a,*], Nerea Bordel [a,*]

[a] University of Oviedo, Department of Physics, Federico García Lorca 18, 33007, Oviedo, Asturias, Spain
[b] Bundesanstalt für Materialforschung und -prüfung (BAM), Richard-Willstätter-Str. 11, 12489 Berlin, Germany

ARTICLE INFO

Keywords:
Laser induced breakdown Spectrocopy (LIBS)
Molecular spectra
Chlorine determination
CaCl emission bands
Industrial gypsum

ABSTRACT

The entire process involving the determination of Cl by molecular emission detection in Laser-Induced Breakdown Spectroscopy (LIBS) is thoroughly studied in this paper. This critical evaluation considers how spectra are normalized, how interferences from other molecular species signals are removed, and how signal integration is applied. Moreover, a data treatment protocol is proposed to achieve reliable and accurate Cl determination from the CaCl molecular spectral signal, not requiring the use of more complex numerical approaches. Calcium chloride dihydrate ($CaCl_2{\cdot}2H_2O$) and high purity anhydrite samples ($CaSO_4$) are used to optimize the acquisition conditions and data treatment of CaCl emission signal. Using the developed protocol, calibration curves for Cl, covering the concentration range from 0 μg/g to 60,000 μg/g of Cl, are successfully achieved. Finally, the suitability of the proposed methodology for Cl determination is successfully applied in industrial gypsum waste samples, where the results obtained by LIBS are validated using high-resolution molecular absorption spectroscopy (HR-CS-MAS) and potentiometric titration.

1. Introduction

Laser-induced breakdown spectroscopy (LIBS) is an analytical technique based on the spectral analysis from a laser-induced plasma, which is typically generated by a high irradiance pulsed laser focused on a sample [1–4]. LIBS is a versatile technique that can be applied to solid, liquid and gaseous samples, either using laboratory equipment, portable devices or remote detection systems. One of the emerging research lines in LIBS is devoted to further improve its sensitivity for the determination of halogens. The detection of these elements by optical emission spectroscopy is especially complex since their resonant lines are located in the ultraviolet vacuum region [5], requiring non-standard detection systems and at vacuum conditions. Alternatively, the detection of halogen atomic IR emission lines, which show weaker emission intensity than the resonant ones, can be enhanced by generating the plasma in a He-rich environment [6–8].

Indirect detection of halogens by LIBS was also investigated using molecular emission from the spectra. In particular, the formation and excitation of diatomic molecules consisting of a halogen and an alkaline earth element is favorable within laser-induced plasmas (LIP) and their molecular emission is observed in the LIBS spectra [9]. This approach is advantageous compared to the one based on the detection of the halogen atomic IR lines since it does not require an external source of He to provide similar or improved limits of detection (LOD) [10–12]. This indirect molecular approach was used for the determination of several halides as F, Cl, Br and I [13–19]. Special attention was paid to Cl quantification since this halogen is a key element in multiple applications, and, specifically, the detection of Cl through CaCl molecular emission was successfully applied in several works. For instance, the presence of Cl is one of the main causes of concrete degradation [20–24]. Moreover, the detection of CaCl was used to obtain information about the minerals present in the Martian soil [25,26] or to assess the degradation of wall paintings in Pompeii [27,28]. Molecular emission was also applied in liquid analysis for the determination of Cl as a pollutant [29].

However, from the different previous studies, it is noticed that there is a non-unified method to determine chlorine in LIBS by CaCl molecular emission:

* Corresponding authors.
E-mail addresses: pisonerojorge@uniovi.es (J. Pisonero), bordel@uniovi.es (N. Bordel).

https://doi.org/10.1016/j.sab.2022.106390
Received 17 January 2022; Received in revised form 18 February 2022; Accepted 18 February 2022
Available online 23 February 2022

- Regarding the spectral range, several studies [20,24]–[26] employed the vibrational bands (sequence $\Delta v = 0$) of the $A\ ^2\Pi \rightarrow X\ ^2\Sigma$ electronic transition, while others [21,23,29] used the sequence $\Delta v = 0$ of the $B\ ^2\Sigma \rightarrow X\ ^2\Sigma$ system.
- Moreover, CaCl emission, in both spectral regions, is strongly interfered by CaO emission. Some authors calculated the interfering CaO contribution by taking the rest of the non-interfering CaO orange system as a reference. Once the CaO contribution was estimated, it could be removed from the integrated signals. For example, this contribution was calculated by performing a partial least squares regression (PLSR) model that took into account the orange CaO emission from 590 to 625 nm [20], or by directly subtracting the CaO intensity adjacent to the CaCl emission [24]. Alternatively, other authors employed baseline correction [23,25], or did not apply any CaO background removal [26,29].
- Normalization methods are often used to deal with the relatively low repeatability of LIBS analysis, since small differences that occur in the initial breakdown conditions imply significant plasma fluctuations [30]. Data normalization was carried out using an internal standard such as the Ca signal [20,29] or the CaOH signal [23]. Other studies evaluated the influence of different normalization procedures on the calibration figures of merit (e.g., LODs, LOQs or R^2) [31,32]. Nevertheless, quantification methods without any normalization process were also employed [25,26].

Therefore, in the present work, a general methodology for the optimization and data treatment of molecular halide compounds is investigated to achieve a proper quantification method. In contrast to previous works, normalization is optimized according to the appearance of the outcoming spectra as the first step in data processing. In particular, the removal of CaO interference is investigated from a spectral point of view (by measuring the spectral profile of CaO and subtracting it from the sample spectrum). Furthermore, it is evaluated how the uncertainty of the calibration is affected by the use of wider or narrower spectral integration ranges. This study is carried out using calcium chloride dihydrate ($CaCl_2{\cdot}2H_2O$) and high purity anhydrite samples ($CaSO_4$). The developed quantification methodology is then applied to samples of industrial interest. Specifically, the proposed procedure is applied to determine Cl in industrial gypsum waste samples, the outcome of desulphurization processes in thermal power plants [33]. The quantification of Cl content in these samples is critical to determine their potential recycling use. The results are validated using other reference analytical techniques such as High Resolution Continuum Source Molecular Absorption Spectroscopy in a graphite furnace (HR-CS-MAS) and potentiometric titration.

2. Experimental

2.1. Chlorine measurements by LIBS

2.1.1. Sample preparation

In this study, calcium chloride dihydrate ($CaCl_2{\cdot}2H_2O$, Sigma Aldrich, Steinheim, Germany) and high purity anhydrite samples ($CaSO_4$, Alpha Aesar, Kandel, Germany), were employed. The sample preparation process involved three main steps: mixing of reagents, drying and pressing. Calibrating samples were obtained by mixing anhydrite samples (5 g) and different amounts of calcium chloride dihydrate to get a Cl concentration range in the samples from 0 μg/g to 60,000 μg/g (micrograms of analyte per grams of sample). To achieve a higher homogeneity in the sample, the mixture of reagents was carried out in wet, dissolving the $CaCl_2{\cdot}H_2O$ in 4 mL of ultrapure water (18.2 MΩ·cm, Milli-Q Synthesis, Merk Millipore, Germany) contained in a beaker. The anhydrite was then added and the resulting paste was mixed with a spatula. The mixture was dried for 24 h at 70 °C in an oven. Sample drying was used to avoid signal depletion due to moisture presence [34,35]. After this process, the sample was crushed in an agate mortar to obtain a homogeneous powder. Finally, the samples were pressed in a hydraulic press (Specac, T-40, Atlas Series Evacuable Pellet Dies), at 10 tons during 60 s, obtaining cylindrical pellets with a diameter of 32 mm and 4 mm thick. Industrial gypsum samples, used to test the developed procedure, were prepared in a similar way but using dried industrial gypsum instead of $CaSO_4$. In this case, different amounts of $CaCl_2{\cdot}2H_2O$ were mixed to obtain added concentrations of Cl from 0 to 5000 μg/g.

2.1.2. Setup

A Q-Switch Nd:YAG 1064 nm laser beam (EKSPLA, NL301HT), operated at 5 Hz, was used as ablation and excitation source. The laser pulse energy was fixed at 100 mJ using an attenuator (LOTIS-TII). The beam was focused on the sample surface through an objective (Thorlabs, LMH-5×-1064, 35 mm focal length). To perform a controlled scan of the sample surfaces, a X-Y platform moved by two stepper motors (PImiCos GmbH VT_80200-2SM and another one manufactured by the University of Oviedo) was used. Plasma emission was collected by two plano-convex lenses (Thorlabs, LA4904-UV and LA4904-UV), forming the plasma image on the spectrograph entrance slit plane. A Czerny-Turner 500 mm focal length spectrograph (Andor Technology, Shamrock SR-500i-D1) coupled to an ICCD (Andor Technology, iStar DH734-25F-03) comprised the detection system. This is a standard experimental system used in other studies, and its scheme was shown in a previous work [36]. The spectrograph was equipped with two gratings of 1200 and 2400 lines/mm respectively. Each spectrum resulted from the accumulation in software of 20 consecutive acquisitions, each one corresponding to an individual laser shot. These 20 shots were made while the sample was moving at 1 mm/s by one of the servomotors, so that in each spectrum the sample was scanned with a 4 mm length raster.

2.2. Chlorine measurements by HR-CS-MAS

2.2.1. Sample preparation

The industrial gypsum (to be analyzed by HR-CS-MAS) was dried overnight at 80 °C. For a practical introduction in the graphite furnace, the sample was prepared as slurry following a modified procedure of Marjanovic et al. [37]. High-purity deionized water with a resistivity of 18 MΩ·cm from a Milli-Q system (Millipore gradient, Merck Millipore, Darmstadt, Germany) was used throughout the experiments. Nitric acid (EMSURE, Merck, Darmstadt, Germany) was used after purification by sub-boiling distillation in perfluoroalkoxy alkanes (PFA) containers. For the slurry of the sample, approximately 100 mg of sample was transferred to 100 mL measuring flask, and 1 mL of concentrated nitric acid and 100 μL glycerin were added. The flask was filled with ultrapure deionized water (18.2 MΩ/cm, Milli-Q Gradient) and sonicated for 10 min in an ultrasonic bath prior to measurement. For statistical propose, this preparation was done by triplicate.

2.2.2. Procedure for measurements

The chloride content in the gypsum sample was indirectly determined by monitoring the band head of the molecular spectrum of the in-situ generated molecule CaCl in a graphite furnace for the electronic transition $A^2\Pi \rightarrow X^2\Sigma$ [38,39]. For this purpose, Ca^{2+} was added as a molecular forming agent from a $Ca(NO_3)_2$ solution. This Ca solution (2.5 g/L in HNO_3, 4%) was made by dissolving $CaCO_3$ (Merk, Certipur, Germany) in nitric acid. A high-resolution continuum source graphite furnace absorption spectrometer ContrAA 800D with PIN platform was employed for the chloride analysis (Analytik Jena GmbH, Jena, Germany). The chloride content in the gypsum sample was measured using external calibration.

2.3. Potentiometric titration

The quantification of chloride was done by using the standardized method of the German Committee for Reinforced Concrete [40], which

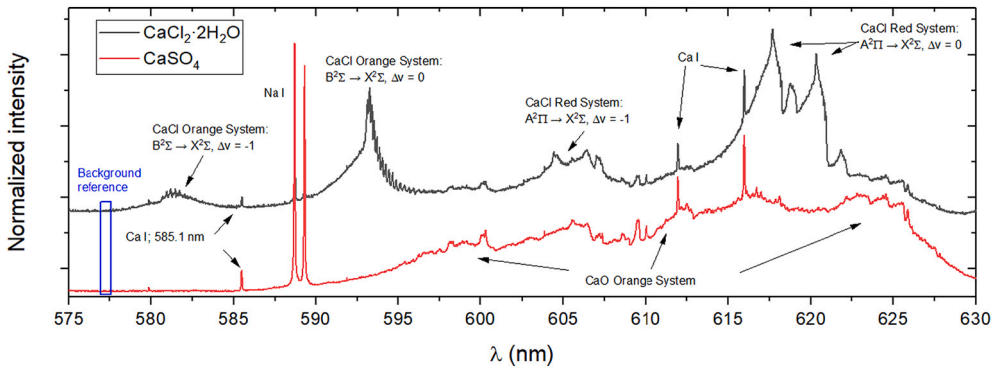

Fig. 1. LIBS spectra obtained from the samples of $CaCl_2{\cdot}2H_2O$ and $CaSO_4$, respectively, with a delay time of 60 μs and a gate of 30 μs. For the $CaSO_4$ spectrum (red), in the whole spectral region from 585 to 630 nm there is a contribution of the CaO signal, although arrows mark only the most intense band heads. (For interpretation of the references to colour in this figure legend, the reader is referred to the web version of this article.)

consist of a potentiometric titration using a $AgNO_3$ solution (Alfa Aesar, 99.9%). 500 mg of the gypsum sample and the cement laboratory standard were refluxed with 20 mL of concentrated HNO_3 during 3 h and then filtrated. The remaining solutions were transferred to 250 mL flasks and filled with water. Each sample was digested and analyzed by triplicate.

3. Results and discussion

3.1. Spectral emission range selection

LIBS spectra from the $CaSO_4$ and $CaCl_2{\cdot}2H_2O$ samples were evaluated to select the most appropriate regions for CaCl detection. Fig. 1 shows the spectra collected, covering the 580–635 nm wavelength

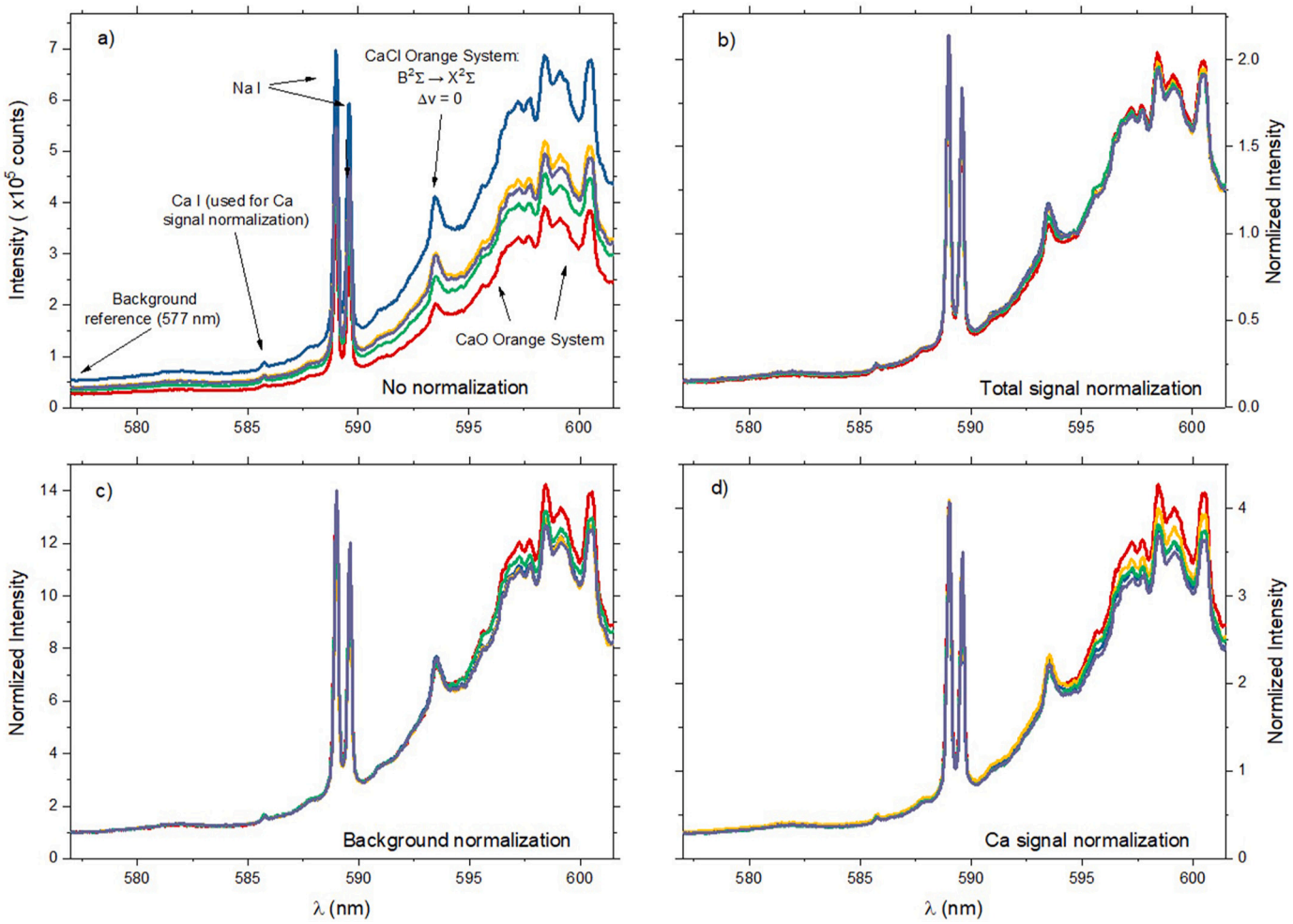

Fig. 2. Comparison of the LIBS spectra obtained (delay 60 μs, gate 200 μs) in each of the 5 repetitions performed on the $CaSO_4$ sample with 1700 μg/g of added Cl: a) non-normalized spectra, b) normalized spectra to total signal (method 1), c) normalized spectra to background (method 2) and d) norminalized spectra to Ca signal (method 3).

range, which resulted from overlapping 4 different exposures (centering the 2400 line/mm diffraction grating at 585, 600, 615 and 630 nm, respectively). The delay and gate acquisition times were set to 60 and 30 μs, respectively, to ensure a significant decay of the atomic signals, obtaining predominantly molecular spectra [11,36]. These arbitrary acquisition times were only used in the first step of the work (spectral range selection). Their optimization is going to be addressed later in the manuscript. In the case of the $CaSO_4$ sample (non Cl containing sample), LIBS molecular spectrum is dominated by CaO emission; while in the case of $CaCl_2{\cdot}2H_2O$ sample, CaCl radical presents strong emission systems in this range [9,41]. Comparing both spectra, it is observed that the CaCl emission is mostly interfered by CaO emission in the different spectral regions. In particular, emission of CaCl observed for the $\Delta v = 0$ and $\Delta v = -1$ transition sequences of the $A^2\Pi \rightarrow X^2\Sigma$ system is strongly interfered with CaO and Ca atomic lines; therefore, they were discarded for quantitative purposes. Alternatively, the $\Delta v = 0$ sequence of the $B^2\Sigma \rightarrow X^2\Sigma$ system (~593 nm) was observed to be only slightly affected by a CaO interference, while the nearest atomic lines (Na, ~589 nm) were relatively far away. Despite the sequence $B^2\Sigma \rightarrow X^2\Sigma$ ($\Delta v = -1$) is free of CaO interference, it was discarded due to its weak intensity as compared to the $B^2\Sigma \rightarrow X^2\Sigma$ ($\Delta v = 0$). Therefore, the $B^2\Sigma \rightarrow X^2\Sigma$ ($\Delta v = 0$) sequence was selected for CaCl detection. After this initial study, spectra were obtained with the 1200 lines/mm grating centered on 593.5 nm, offering a wider spectral range, of approximately 30 nm (i.e., 577–610 nm) in a single exposition.

3.2. Normalization procedure and background definition

Prior to any normalization process, the contribution of the dark current (measured under the same conditions of acquisition but without generating plasma) was subtracted to all the spectra. It has to be remarked that even if the background intensity due to dark current is small (~$4{\cdot}10^3$counts) compared to the background recorded with plasma (~10^5counts), it may turn significant when applying correction factors to the spectra, since it is a constant contribution independent of any plasma conditions variation and therefore it should not be considered for normalization purposes.

In relation to normalization procedures, 3 methods were studied including normalizing to the total emission intensity of the spectrum registered in the ICCD (method 1), normalizing to the background (method 2), and normalizing to the signal of a Ca emission line, i.e., internal standard, (method 3). These 3 methods were chosen to keep a unified normalization criterion for the spectra of all samples, so the selected parameters are supposed to remain constant regardless the differences that may exist between samples. Specifically, considering that the main difference between the samples was the amount of additive ($CaCl_2{\cdot}2H_2O$), parameters were chosen in such a way that they were not highly dependent on the concentration of this compound. On the one hand, normalization to Ca was tested since the variations of Ca content were negligible when adding small amounts of $CaCl_2{\cdot}2H_2O$ to a CaO_4 matrix. On the other hand, normalization to total signal was revealed like CaO signal normalization since this emission dominates the spectra, and its concentration is supposed to be constant among the samples. Nevertheless, normalization to Na lines was not tested since Na is a trace element in the additive. Therefore, the Na signal is a variable parameter among the samples so that the normalization method would not be homogeneous. In all the cases, the normalization procedure consists of dividing one by one all the intensities along the spectrum by a constant factor, which is specific for each spectrum and depends on the normalization method. In method 1, the correction factor represents the integrated emission all over the 1024 pixels of the spectrum (wavelengths from 577 to 610 nm). Method 2 uses the average intensity recorded between 577.10 and 577.50 nm as a normalization factor associated with the continuous emission background, as shown in Fig. 1. In method 3, the correction factor is the intensity of the Ca I emission line at 585.75 nm (internal standard) which is obtained by integrating the spectrum between 585.5 and 586 nm, subtracting the area under the baseline.

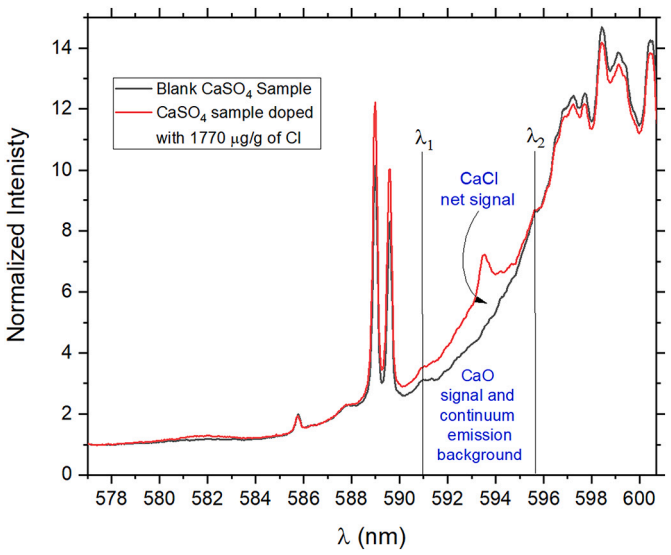

Fig. 3. Normalized average spectra from the $CaSO_4$ sample (blank) and $CaSO_4$ sample with 1770 μg/g of added Cl (red), both measured under the same conditions (delay of 50 μs and gate of 100 μs). The superposition of these two spectra allows graphically defining the net CaCl signal, and both the CaO signal and the emission continuum that form the background. (For interpretation of the references to colour in this figure legend, the reader is referred to the web version of this article.)

Fig. 2(a) shows LIBS spectra (5 consecutive acquisitions) after dark current removal without any kind of normalization, obtained from the $CaSO_4$ sample doped with 1770 μg/g of Cl. The inherent high variability on the LIBS emission signals is noticeable, evidencing the need for normalization procedures. The normalized spectra obtained by the three methods described above are plotted in Fig. 2(b), (c) and (d), respectively. It is observed that method 1 achieves a greater reproducibility for the CaO emission signal, which is the one that predominates in the spectrum. However, method 2 should be considered as the most appropriate normalization method since it minimizes the variability of the CaCl signal, which will be employed for quantification purposes.

Once the signals were normalized, net signal for CaCl emission bands was obtained using eq. 1:

$$S_{net} = S_{tot} - S_b \quad (1)$$

where S_{net} is the net signal of CaCl, S_{tot} is the total integrated signal between the selected spectral limits and S_b is the background integrated signal between those limits.

One of the main issues when handling spectra of diatomic molecules formed by an alkaline earth and a halogen is the proper definition of the background. This is because alkaline earth-halogen emission spectra is often interfered with the alkaline earth-oxygen emission signals [9]. Oxygen might be present in the sample or can be incorporated from the atmosphere at which the LIBS experiment is carried out. In this context, the background definition takes into account the contribution of the background emission continuum and the contribution of the CaO emission bands. This emission cannot be removed, for example, by generating the plasma in an O-free atmosphere, since the concentration of this element is very high in the sample itself. In this work, the use of a blank sample (containing no Cl) was evaluated to remove the contribution of both the CaO interference and the continuous background. Fig. 3 shows the normalized spectra (using method 2) obtained for the $CaSO_4$ sample containing 1770 μg/g Cl and for the blank. It is found that normalization makes the blank spectrum properly fit the spectral basis of the CaCl signal, so background emissions can be spectrally removed to get the CaCl net signal.

Table 1
Spectrum acquisition conditions evaluated for the delay time optimization. (*) Note that for the 80 μs series it was necessary to increase the ICCD gain from 0 to 16% to acquire enough signal.

Delay time (μs)	Gate time (μs)
20	5
30	9
40	20
50	100
60	200
80	200*

As previously discussed, S_b involves both the CaO interference and the continuum background, which are determined by the blank spectrum (see labels for CaO background signal and continuum background in Fig. 3). Therefore, this procedure allows obtaining the net CaCl signal by spectrally subtracting the blank signal from the sample signal. It should be remarked that the fit of the blank spectrum is not optimal over the whole spectral range shown in Fig. 3: regions close to Na lines (~589 nm) or the most intense CaO range (~599 nm) show slight differences between the two spectra. Nevertheless, it is possible to define a region close to the CaCl emission (labels λ_1-λ_2 in Fig. 3), where the fitting is optimal for quantification purposes, an issue that will be addressed later in the manuscript.

3.3. Acquisition delay time optimization

Among the different LIBS acquisition parameters, delay time was carefully optimized. It is known that the temporal evolution of a LIP plasma causes different sequential ionic, atomic or molecular radiation to predominate in the spectral emission [1]. For the specific case of molecular signal detection, several authors propose the use of long enough delay times so that the atomic signals decay while the molecular signals, which are more persistent, predominate. However, for CaCl detection, not only the decay of the atomic signal needs to be taken into account but also the dynamics of both molecular CaCl and CaO emissions, being the latter the main source of interference. To evaluate the optimal conditions, spectra were measured at different delay times; and for each one, the gate time was tuned to achieve the maximum spectral signal on the ICCD avoiding saturation (i.e., not exceeding 40,000 counts for the maximum of the CaO emission at ~599 nm). The acquisition conditions, detailed in Table 1, were applied to obtain spectra from the $CaSO_4$ sample with 1770 μg/g of added Cl.

As can be seen in Fig. 4(a), the different temporal evolution of the molecular emission signals makes the normalized CaCl signal enhanced with respect to the CaO when increasing the delay acquisition time. Net CaCl signals corresponding to each delay time were obtained subtracting the blank spectrum to each sample spectrum measured under the same delay time, integrating the resulting spectra between 592.80 (λ_1) and 594.20 nm (λ_2). Fig. 4(b) shows in a bar-graph the evolution of the net CaCl signal at increasing delay times. Uncertainties associated with the measured net CaCl signal involve both the error from the measurement of the Cl-containing sample and the error from the blank measurement. It is noticed that the net CaCl signal increases with delay, stabilizing from 50 μs onwards. However, the increase of the delay might lead to an increase in the uncertainty. Therefore, in terms of measurement reliability, it would not be adequate to use too long delay times. In this work, 50 μs of was chosen as optimal delay time, balancing a relatively high net CaCl signal with a relatively low uncertainty.

3.4. Calibration procedure

The set of $CaSO_4$ calibrating samples, ranging from a concentration of 0% to 6% of Cl, was measured under optimized acquisition conditions (delay of 50 μs and gate of 100 μs). The analyses involved 7 repetitions, obtaining 7 spectra per sample. In particular, each spectrum was treated according to normalizing method 2, which involves the subtraction of the dark current and the normalization to emission background. Fig. 5 (a) shows the normalized spectra obtained for each calibrating sample. As can be seen, the blank sample spectrum properly fits the basis of the CaCl signals of all samples. Then, the average normalized blank spectrum was subtracted from each individual calibration sample spectrum. It should be noted that this process was applied to each one of the 7 spectra taken in each sample (one per repetition). Fig. 5 (b) shows each averaged sample spectrum after blank subtraction. Na lines at 589 nm,

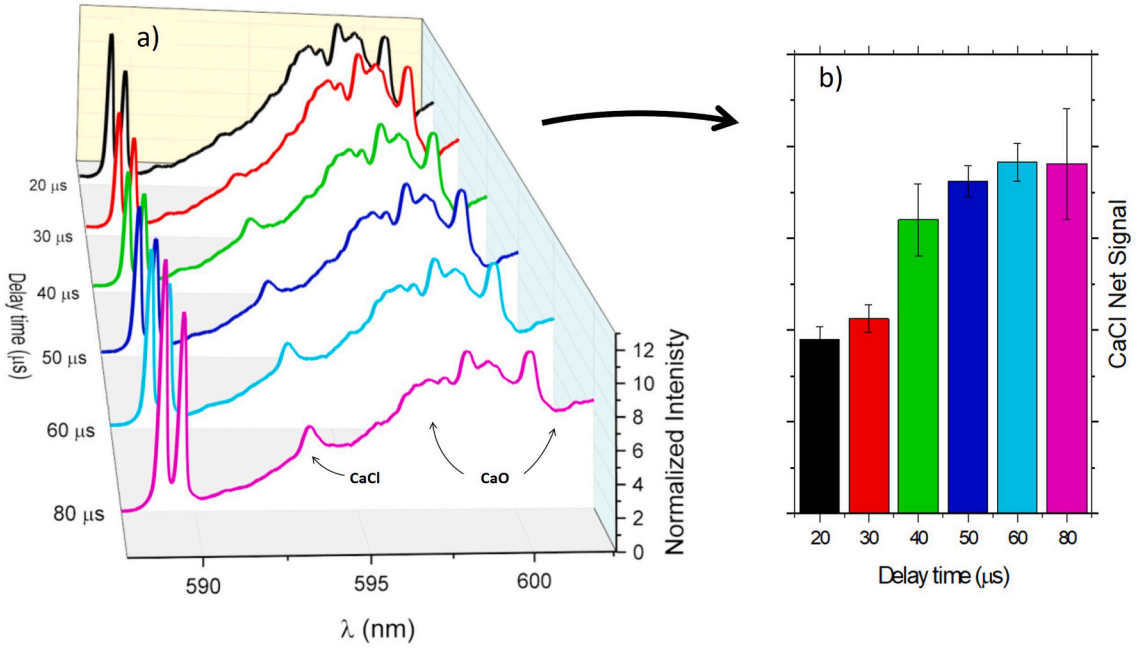

Fig. 4. a) Average spectra obtained on the $CaSO_4$ sample with 1770 μg/g of added Cl measured at different delay times, after applying normalization to the background (method 2). b) Net CaCl signal integrated in the range (λ_1-λ_2) = 592.80–594.20 nm for each one of the measured delay times.

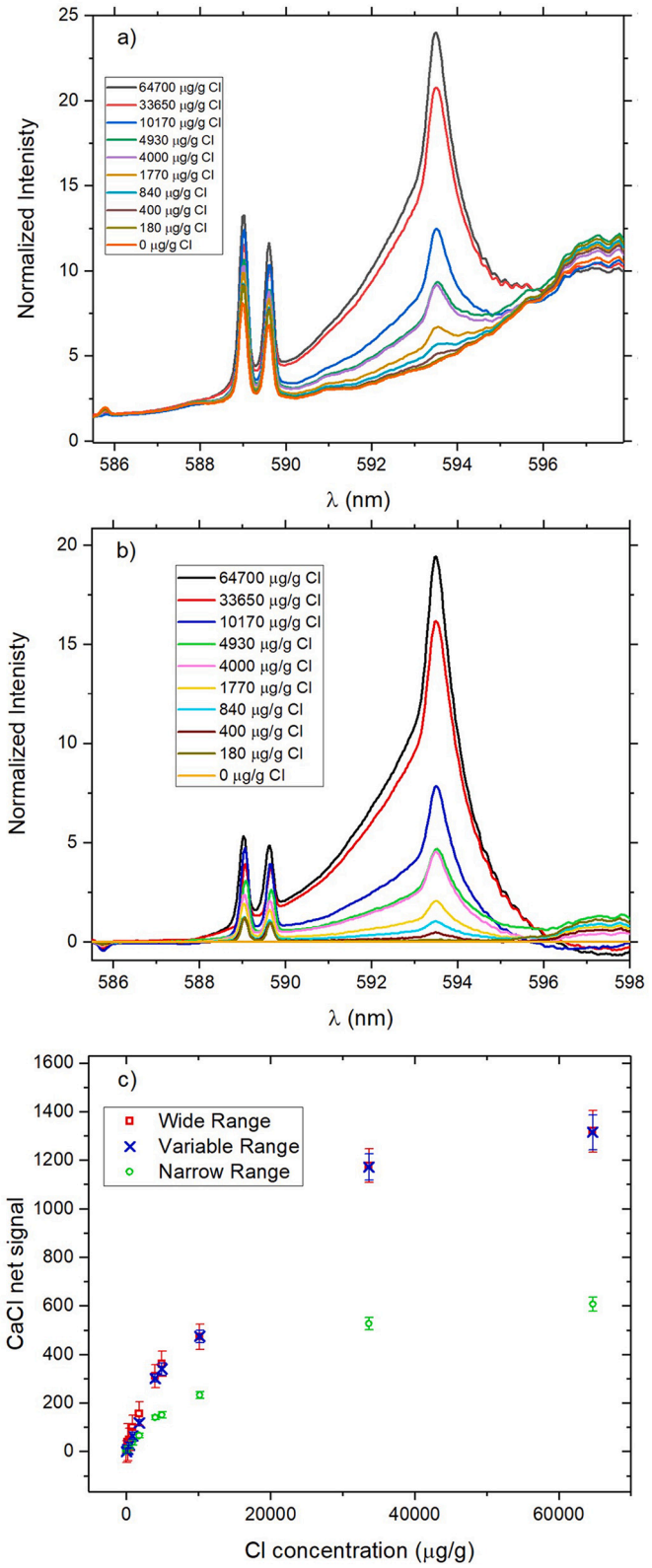

Fig. 5. a) Average normalized spectra from each one of the analyzed anhydrite samples, measured with a delay time of 50 µs and gate width of 100 µs. b) Same spectra after blank spectrum subtraction. C) Calibration curve for the whole set of samples using the wide, variable and narrow integration ranges.

Table 2
List of the integration limits employed as well as the samples to which they are applied.

Integration Range	Analyzed anhydrite samples	Integration limits (nm)
Narrow	All	592.8–594.2
Wide	All	587.9–596.1
Variable	64,700 µg/g of Cl	587.9–596.1
	33,650 µg/g of Cl	587.9–596.1
	10,170 µg/g of Cl	588.3–595.5
	4930 µg/g of Cl	588.3–595.5
	4000 µg/g of Cl	588.3–595.5
	1770 µg/g of Cl	590.9–594.9
	840 µg/g of Cl	591.5–594.9
	400 µg/g of Cl	591.5–594.2
	180 µg/g of Cl	592.5–594.2
	0 µg/g of Cl	592.5–594.2

CaCl molecular emission and some CaO emission at higher wavelengths than 596 nm are observed in the spectra.

The extension of the CaCl molecular emission bands of the $\Delta v = 0$ sequence on each sample, should be considered when selecting the integration range of the CaCl signal, since a larger integration range including all the spectral emission improves the sensitivity of the calibration. For instance, the samples with the highest Cl concentration (64,700 µg/g) show a CaCl molecular emission covering 8 nm (~588–596 nm). However, if such a large integration range is employed, fluctuations in the background will increase the uncertainty in the integrated signal for the samples with low Cl content, in which CaCl is only visible between 593 and 594 nm. Thus, the influence of the integration range (λ_1-λ_2) was evaluated in terms of uncertainty, sensitivity (linear regression slope), linearity (correlation coefficient R^2) and limit of detection (LOD). For this purpose, net normalized CaCl spectra (after blank subtraction) obtained for the calibration samples were integrated using 3 different wavelength ranges: "wide range", which covers from 587.9 to 596.1 nm; "narrow range", which covers from 592.8 to 594.2 nm; and "variable range", which is selected depending on the extension of the CaCl emission for each sample. These "variable ranges" are defined by the two closest wavelengths to 593.5 nm, whose intensities are below the 8% of the maximum intensity of the CaCl (measured at 593.5 nm). If this condition is fulfilled under the Na lines, the initial integration limit is fixed at the beginning of the Na lines. In the cases in which the Na emission is included within the integration range, the contribution of these lines is removed by using a baseline under the lines. In addition, the ranges for the samples with no visible CaCl signal, for example the blank, are the same as for the sample with the minimum visible CaCl emission. Table 2 lists the integration limits of these wavelength ranges. Note that the Na emission lines are included within several of these integration ranges, but their contribution was removed by employing a baseline between 588.3 and 590.2 nm.

Uncertainties associated to each value (S_{net}) were calculated considering uncertainty propagation as indicated in eq. 2:

$$\delta S_{net}(i) = \sqrt{\delta S_{tot}(i)^2 + \delta S_b^2} \quad (2)$$

where $\delta S_{net}(i)$ is the uncertainty associated with the integrated net CaCl signal of the i^{th} sample, $\delta S_{tot}(i)$ is the standard deviation of the integrated signal into the 7 repetitions taken from the i^{th} sample, and δS_b is the standard deviation of the total signal integrated into the spectrum of the blank sample. Fig. 5(c) plots the integrated net CaCl signal versus Cl concentration, using the wide, variable and narrow integration ranges. It is observed that at high Cl concentrations the emission signal tends to an asymptotic behavior, while at lower concentrations (< 5000 µg/g) a linear response is found. This linear dynamic range observed in the calibration curve is lower compared to other matrices, such as cement, in which the linear calibrations cover ranges of up to 2% of Cl [20,21,23]–[25]. The formation of CaCl depends on the concentration of both Ca and Cl, and therefore, only when the amount of Ca is much

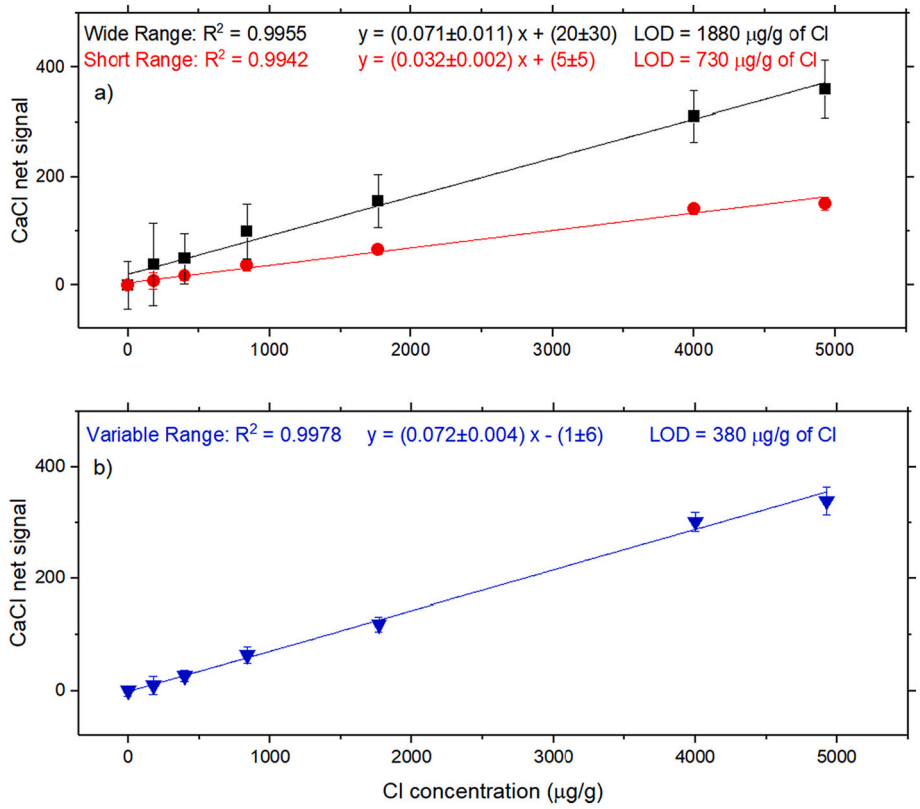

Fig. 6. Calibration curves with their corresponding linear fittings, obtained on samples with a concentration lower than 5000 µg/g of Cl. In a) the results for the two fixed integration ranges are shown, and in b) those corresponding to the variable integration range.

higher than the amount of the halogen in the plasma, signal variations in the molecular bands can be associated with the variation of the halogen content. In this line, previous studies reported limitations on the calibration of halogens by diatomic molecular emission detection (e.g. CaF, CaCl) in LIBS [11,26], showing that linearity is lost when the amount of Ca is not high enough. The fact that $CaSO_4$ matrix exhibits a limited dynamic range in the calibration of Cl concentration could be attributed to relatively lower availability of Ca, since anhydrite contains a high O concentration, which captures a large part of the Ca available in the sample to form CaO. Moreover, self-absorption of the CaCl emission at high Cl concentrations cannot be either discarded to explain this asymptotic behavior [25].

The fitting calibration lines were therefore obtained for the samples with Cl concentrations up to 5000 µg/g. Fig. 6(a) shows the calibration curves calculated for the "narrow" and "wide" integration ranges and Fig. 6(b) that for the "variable". Regarding sensitivity, it is found that the narrow integration range offers the smallest slope, since a restricted region of the entire available CaCl signal is being integrated. However, for the variable and wide ranges, a similar slope is found since the entire CaCl emission is being integrated. With respect to the uncertainty of the data points, it is maximized when the wide range of integration is used, meanly for low Cl concertation samples, due to the fact that a range of the spectrum which is being integrated is not actually CaCl signal but background emission. For instance, in Fig. 5(b) it is noticed that at low Cl concentrations, the CaCl signal is only visible between 593 and 594 nm, while wide range integration comprises the integration from 587.9 to 596.1 nm. This high uncertainty is significantly reduced when integrating with the variable range, since the integration of each spectrum is set to the entire available CaCl signal. Linearity (R^2) remains similar, no relevant changes are observed regardless of the integration range. Then, taking into account the slope (m) and the uncertainty in the net signal of the blank (δS_b) for each integration range calibration, the LODs can be calculated as:

Table 3
List of employed samples within the industrial gypsum standard addition analysis, as well as the integration limits applied for each sample.

Analyzed gypsum samples	Integration limits (nm)
5220 µg/g of added Cl	587.5–595.7
4300 µg/g of added Cl	587.5–595.7
3350 µg/g of added Cl	587.5–595.7
1910 µg/g of added Cl	587.5–595.7
1110 µg/g of added Cl	587.5–595.0
0 µg/g of added Cl	587.5–595.0

$$LOD = \frac{3\,\delta S_b}{m} \tag{3}$$

LODs of 1880, 730 and 380 µg/g of Cl are obtained for the wide, narrow and variable integrations ranges, respectively. The LOD values for the wide and narrow ranges are not realistic, since, as can be seen from the spectra in Fig. 5(a) and (b), the signal coming from the sample containing 400 µg/g of Cl is clearly distinguishable from the blank. Nevertheless, the LOD (380 µg/g) for the variable range is more reliable, adequately matching that observed in the spectra of Fig. 5(b).

3.5. Application test

Finally, the developed methodology was applied for the determination of Cl mass content in industrial gypsum samples. A calibration by means of standard additions was used for this purpose. Table 3 lists the different amounts of Cl that were added to the test sample. Spectra of these calibrating samples were obtained at the same conditions as those employed for the analysis of anhydrite samples (i.e., delay 50 µs, gate 100 µs, see Fig. 5) and were normalized to spectral background (method 2) after dark current subtraction. In the particular case of the standard

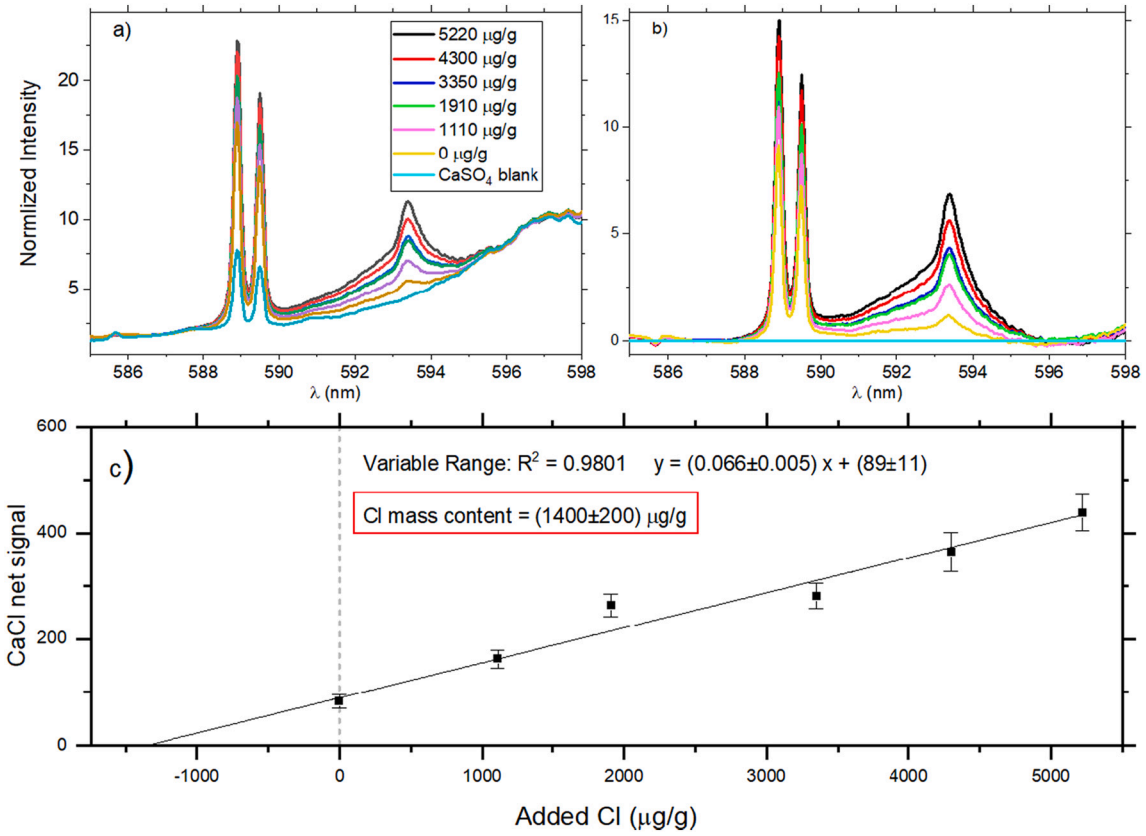

Fig. 7. a) Average normalized spectra from the industrial gypsum samples, each one containing a certain amount of added Cl (see legend). The last series is the spectrum of the $CaSO_4$ blank sample. Spectra were taken at a delay time of 50 µs and gate width of 100 µs. b) Same spectra after blank spectrum subtraction, which represent the net CaCl signal. c) Calibration curve for set of samples.

additions, no blank sample is available, but, as can be seen in Fig. 7(a), the spectrum from the anhydrite blank can be used for background removal as it properly fits the CaO emission appearing under the CaCl bands. As discussed in the previous section, a variable range was used for emission integration (see Table 3). Since higher Na signals are measured in the industrial samples, the baseline taken to remove the contribution of these lines was extended from 587.6 to 590.8 nm.

The application of this quantitative method resulted in a calculated Cl mass content in the sample of 1400 ± 200 µg/g. This value was validated by analyzing the industrial gypsum sample with two alternative techniques: potentiometric titration and HR-CS-MAS. The results obtained are, respectively, 1540 ± 20 and 1490 ± 120 µg/g of Cl. All three results are within the error range given by the uncertainties, so it is considered a valid result. Therefore, the outcome confirms that the developed methodology is applicable for determining Cl in gypsum from thermal power plants.

4. Conclusions

In this work, all processes involved in determining the Cl mass concentration in anhydrite and industrial gypsum waste matrices by molecular LIBS spectroscopy are reviewed in detail. It is shown that, after the subtraction of dark current, the application of a normalization factor to all the intensities of the spectrum enables the comparison of spectra taken under the same conditions. In fact, the correction factor obtained from the continuous emission background is the one that best compensates for the spectral CaCl intensity variations. Moreover, the best procedure for the removal of the CaO interference in the CaCl signals is the spectral superposition of a blank sample spectrum taken under the same conditions. It is shown that late detection yields more predominant CaCl signals. However, the uncertainty in the CaCl signal also increases with delay, so the setting of this parameter involves a compromise between signal enhancement and signal error. Finally, it is noticed that variable integration ranges provide high sensitivity while reducing the uncertainties in the determination of the net CaCl signal. Calibration curves maintain linearity for Cl concentrations up to 5000 µg/g, demonstrating that this method makes possible a reliable determination of the Cl concentration in calcium sulfate matrices. In addition, the proposed methodology was successfully applied for the determination of Cl mass content in industrial gypsum waste. The content of 1400 µg/g of Cl obtained by a standard addition calibration is in accordance with the results determined by other reference techniques such as high-resolution molecular absorption spectroscopy and potentiometric titration.

The experimental system employed on this work could be implemented in an industrial facility as an off-line technique. It was shown that, a low-cost technique like LIBS, is able to accurately quantify Chlorine in samples of industrial interest. The total duration of the analysis is determined by the time required to dry and press the sample to form the pellets, with no additional sample preparation needed. In this line, further efforts are still necessary to make a feasible online LIBS system for Cl determination in high-moisture content gypsum samples.

Declaration of Competing Interest

The authors declare no conflict of interest

Acknowledgements

The authors gratefully acknowledge the financial support of the Spanish Government through the projects MINECO 17-CTQ2016-77887-C2-1R and MCI-21-PID2020-113951GB-100, the pre-doctoral

grant MINECO BES-2017-080768. Financial support from the Government of the Principality of Asturias (Fondos Feder) through the project GRUPIN IDI-2018-000186, and pre-doctoral grants PAPI-20-PF-03 and PA-21-PF-BP20-059 is also recognized.

The assistance provided by the Scientific-Technical Services (SCTs) of the University of Oviedo, through its technicians Beatriz Ramajo, Azucena Lara-Gonzalo and Beatriz Gutierrez, is also gratefully acknowledged.

References

[1] D.A. Cremers, L.J. Radziemski, Handbook of Laser-Induced Breakdown Spectroscopy, John Wiley & Sons, Ltd, Chichester, UK, 2006.
[2] D.W. Hahn, N. Omenetto, Laser-induced breakdown spectroscopy (LIBS), part I: Review of basic diagnostics and plasmaparticle interactions: Still-challenging issues within the analytical plasma community, Appl. Spectrosc. 64 (12) (2010).
[3] D.W. Hahn, N. Omenetto, Laser-induced breakdown spectroscopy (LIBS), part II: review of instrumental and methodological approaches to material analysis and applications to different fields, Appl. Spectrosc. 66 (4) (Apr. 2012) 347–419.
[4] R.E. Russo, X.L. Mao, J.H. Yoo, J.J. Gonzalez, Laser ablation, Laser-Induced Break. Spectrosc. (Jan. 2007) 49–82.
[5] D.E. Anderson, et al., Characterization of LIBS emission lines for the identification of chlorides, carbonates, and sulfates in salt/basalt mixtures for the application to MSL ChemCam data, J. Geophys. Res. Planets 122 (4) (Apr, 2017) 744–770.
[6] M. Tran, Q. Sun, B.W. Smith, J.D. Winefordner, Determination of F, Cl, and Br in solid organic compounds by laser-induced plasma spectroscopy, Appl. Spectrosc. 55 (6) (Jun. 2001) 739–744.
[7] D.A. Cremers, L.J. Radziemski, Detection of chlorine and fluorine in air by laser-induced breakdown spectrometry, Anal. Chem. 55 (8) (Jul. 1983) 1252–1256.
[8] L. St-Onge, E. Kwong, M. Sabsabi, E.B. Vadas, Quantitative analysis of pharmaceutical products by laser-induced breakdown spectroscopy, Spectrochim. Acta - Part B At. Spectrosc. 57 (7) (Jul. 2002) 1131–1140.
[9] M. Gaft, L. Nagli, N. Eliezer, Y. Groisman, O. Forni, Elemental analysis of halogens using molecular emission by laser-induced breakdown spectroscopy in air, *Spectrochim.* Acta - Part B At. Spectrosc. 98 (June) (2014) 39–47.
[10] C. Álvarez, J. Pisonero, N. Bordel, Quantification of fluorite mass-content in powdered ores using a Laser-Induced Breakdown Spectroscopy method based on the detection of minor elements and CaF molecular bands, *Spectrochim.* Acta - Part B At. Spectrosc. 100 (Oct. 2014) 123–128.
[11] C. Alvarez-Llamas, J. Pisonero, N. Bordel, Quantification of fluorine traces in solid samples using CaF molecular emission bands in atmospheric air LIBS, *Spectrochim.* Acta - Part B At. Spectrosc. 123 (Sep. 2016) 157–162.
[12] C. Alvarez-Llamas, J. Pisonero, N. Bordel, A novel approach for quantitative LIBS fluorine analysis using CaF emission in calcium-free samples, J. Anal. At. Spectrom. 32 (1) (2017) 162–166.
[13] O. Forni, et al., First detection of fluorine on Mars: implications for Gale Crater's geochemistry, Geophys. Res. Lett. 42 (4) (Feb. 2015) 1020–1028.
[14] M. Gaft, L. Nagli, I. Gornushkin, Y. Raichlin, Review on recent advances in analytical applications of molecular emission and modelling, Spectrochimica Acta - Part B Atomic Spectrosc. 173 (01-Nov-2020) 105989. Elsevier B.V.
[15] M. Gaft, L. Nagli, Y. Raichlin, F. Pelascini, G. Panzer, V.M. Ros, Laser-induced breakdown spectroscopy of Br and I molecules with alkali-earth elements, Spectrochim. Acta - Part B At. Spectrosc. 157 (Jul. 2019) 47–52.
[16] M. Resano, et al., Breaking the boundaries in spectrometry. Molecular analysis with atomic spectrometric techniques, TrAC - Trends Analyt. Chem. 129 (2020).
[17] Q. Li, et al., Determination of fluorine content in rocks using laser-induced breakdown spectroscopy assisted with radical synthesis, Talanta 234 (Nov. 2021), 122712.
[18] C. Méndez-López, et al., Laser induced plasmas at different nebulization conditions: Spatio-temporal distribution of emission signals and excitation temperatures, Spectrochim. Acta - Part B At. Spectrosc. 170 (Aug. 2020).
[19] M. Oujja, J.J. Camacho, D. Paradela, M. Castillejo, R. de Nalda, Emission characteristics and dynamics of neutral, ionic and molecular species in a laser produced CaF2 plasma, J. Quant. Spectrosc. Radiat. Transf. 276 (Dec. 2021).
[20] W. Zhang, et al., Determination of chlorine with radical emission using laser-induced breakdown spectroscopy coupled with partial least square regression, Talanta 198 (Jun. 2019) 93–96.
[21] N. Omenetto, W.B. Jones, B.W. Smith, T. Guenther, E. Ewusi-Annan, U. of Florida, Feasibility of Atomic and Molecular Laser Induced Breakdown Spectroscopy (LIBS) to In-Situ Determination of Chlorine In Concrete : Final Report, Oct. 2016.
[22] S. Millar, C. Gottlieb, T. Günther, N. Sankat, G. Wilsch, S. Kruschwitz, Chlorine determination in cement-bound materials with Laser-induced Breakdown Spectroscopy (LIBS) – A review and validation, *Spectrochim.* Acta - Part B At. Spectrosc. 147 (Sep. 2018) 1–8.
[23] T. Dietz, J. Klose, P. Kohns, G. Ankerhold, Quantitative determination of chlorides by molecular LIBS, *Spectrochim.* Acta - Part B At. Spectrosc. 152 (Feb. 2019) 59–67.
[24] M.A. Wakil, Z.T. Alwahabi, Microwave-assisted laser induced breakdown molecular spectroscopy: quantitative chlorine detection, J. Anal. At. Spectrom. 34 (9) (Sep. 2019) 1892–1899.
[25] D.S. Vogt, K. Rammelkamp, S. Schröder, H.W. Hübers, Molecular emission in laser-induced breakdown spectroscopy: an investigation of its suitability for chlorine quantification on Mars, Icarus 302 (Mar. 2018) 470–482.
[26] D.S. Vogt, S. Schröder, K. Rammelkamp, P.B. Hansen, S. Kubitza, H.-W. Hübers, CaCl and CaF emission in LIBS under simulated Martian conditions, Icarus 335 (Jan. 2020), 113393.
[27] S. Pérez-Diez, et al., Elucidation of the chemical role of the pyroclastic materials on the state of conservation of mural paintings from Pompeii, Angew. Chem. Int. Ed. 60 (6) (Dec. 2021) 3028–3036.
[28] S. Pérez-Diez, et al., Chemometrics and elemental mapping by portable LIBS to identify the impact of volcanogenic and non-volcanogenic degradation sources on the mural paintings of Pompeii, Anal. Chim. Acta 1168 (Jul. 2021), 338565.
[29] Z. Tang, et al., Sensitive analysis of fluorine and chlorine elements in water solution using laser-induced breakdown spectroscopy assisted with molecular synthesis, Talanta 224 (Mar. 2021), 121784.
[30] Y.T. Fu, et al., Mechanism of signal uncertainty generation for laser-induced breakdown spectroscopy, Front. Phys. 16 (2) (Apr. 2021) 1–10.
[31] J. Guezenoc, A. Gallet-Budynek, B. Bousquet, Critical review and advices on spectral-based normalization methods for LIBS quantitative analysis, Spectrochimica Acta - Part B Atomic Spectrosc. 160 (01-Oct-2019) 105688. Elsevier B.V.
[32] E. Tognoni, G. Cristoforetti, Signal and noise in Laser Induced Breakdown Spectroscopy: An introductory review, Opt. Laser Technol. 79 (01-May-2016) 164–172. Elsevier Ltd.
[33] N.H. Koralegedara, P.X. Pinto, D.D. Dionysiou, S.R. Al-Abed, Recent advances in flue gas desulfurization gypsum processes and applications – A review, J. Environ. Manag. 251 (01-Dec-2019) 109572. Academic Press.
[34] B. Bousquet, et al., Development of a mobile system based on laser-induced breakdown spectroscopy and dedicated to in situ analysis of polluted soils, *Spectrochim.* Acta - Part B At. Spectrosc. 63 (10) (2008) 1085–1090.
[35] V.N. Lednev, et al., Combining Raman and laser induced breakdown spectroscopy by double pulse lasing, Anal. Bioanal. Chem. 410 (1) (Jan. 2018) 277–286.
[36] L.J. Fernández-Menéndez, C. Méndez-López, C. Alvarez-Llamas, C. González-Gago, J. Pisonero, N. Bordel, Spatio-temporal distribution of atomic and molecular excited species in laser-induced breakdown spectroscopy: potential implications on the determination of halogens, Spectrochim. Acta - Part B At. Spectrosc. 168 (Jun. 2020).
[37] L. Marjanovic, R.I. McCrindle, B.M. Botha, J. Hermanus Potgieter, Analysis of cement by inductively coupled plasma optical emission spectrometry using slurry nebulization, J. Anal. At. Spectrom. 15 (8) (Aug. 2000) 983–985.
[38] M.A. Bechlin, E.C. Ferreira, J.A. Gomes Neto, Determination of chlorine in cement via CaCl molecule by high-resolution continuum source graphite furnace molecular absorption spectrometry with direct solid sample analysis, Microchem. J. 132 (May 2017) 130–135.
[39] A. Guarda, M. Aramendía, I. Andrés, E. García-Ruiz, P.C. Do Nascimento, M. Resano, Determination of chlorine via the CaCl molecule by high-resolution continuum source graphite furnace molecular absorption spectrometry and direct solid sample analysis, Talanta 162 (Jan. 2017) 354–361.
[40] DAfStb-Heft 401: 1989, Instructions for the Determination of the Chloride Content of Concrete, Beuth, Berlin, 1989.
[41] R.W.B. Pearse, A.G. Gaydon, The Identification of Molecular Spectra, Chapman & Hall, 1976.